

Fabrication of Er³⁺-doped LaOCl nanostructures with upconversion and near-infrared luminescence performances

Wensheng Yu · Qingling Kong · Jinxian Wang ·
Xiangting Dong · Guixia Liu

Received: 10 September 2013 / Accepted: 10 October 2013 / Published online: 25 October 2013
© Springer Science+Business Media New York 2013

Abstract LaOCl:Er³⁺ nanofibers and nanobelts were prepared by electrospinning combined with a double-crucible chlorination technique using NH₄Cl powders as chlorinating agent. X-ray powder diffraction analysis indicated that LaOCl:Er³⁺ nanostructures were tetragonal with space group P4/nmm. Scanning electron microscope analysis and histograms revealed that diameter of LaOCl:Er³⁺ nanofibers and the width of nanobelts respectively were 161.15 ± 18.11 nm and 6.11 ± 0.19 μm under the 95 % confidence level, and the thickness of nanobelts was 116 nm. Up-conversion (UC) emission spectra analysis manifested that LaOCl:Er³⁺ nanostructures exhibited strong green and red UC emission centering at 525, 548 and 671 nm, respectively attributed to ²H_{11/2} → ⁴I_{15/2}, ⁴S_{3/2} → ⁴I_{15/2} and ⁴F_{9/2} → ⁴I_{15/2} energy levels transitions of Er³⁺ ions under the excitation of a 980-nm diode laser. It was found that the relative intensities of green and red emissions vary obviously with the changing of concentration of Er³⁺ ions, and the optimum molar percentage of Er³⁺/(La³⁺+Er³⁺) ions was 5 % in the LaOCl:Er³⁺ nanostructures. The LaOCl:x %Er³⁺ nanobelts have higher UC emission (both red and green) intensity than the counterpart nanofibers. Moreover, the near-infrared characteristic emissions of LaOCl:Er³⁺ nanostructures were achieved under the excitation of a 532-nm laser. Commission Internationale de L'Eclairage analysis demonstrated that color-tuned luminescence can be obtained by

changing doping concentration of Er³⁺ ions, which could be applied in the fields of optical telecommunication and optoelectronic devices. The UC luminescent mechanism of LaOCl:Er³⁺ nanostructures were also proposed.

1 Introduction

In the last few decades, rare-earth doped upconversion luminescent materials have attracted much interest for their potential applications in many areas such as all-solid compact lasers, near infrared quantum counting devices, optical data storage, fluorescent labels for sensitive detection of bimolecular [1–5], and especially bioprobes and bioimages [6, 7]. Among the up-conversion (UC) luminescent rare-earth ions, the Er³⁺ is an ideal candidate for upconversion since its metastable level ⁴I_{11/2} can be conveniently populated by a 980-nm diode laser, which can exhibit green and red visible emission [8]. The dynamics of the excited states of rare earth ions can be controlled by selecting different host materials [9, 10]. The host materials with low phonon energy can result in a reduction of the multiphonon relaxation and thus help efficient upconversion occur. Lanthanum oxychloride (LaOCl) is known for the high chemical stability, nontoxicity, the low maximum phonon cutoff energy, and ability to promote efficient phonon energy transfer (ET) to dopant ions, which are originated from the low phonon vibrational energy and high ionicity of the bond between rare earth and chlorine [11]. Its structure comprises distinct covalent (LaO)_n⁺ complex cation and Cl⁻ anion layers. In this structure, the La³⁺ is coordinated with four oxygens and five chlorines forming a monocapped tetragonal antiprism arrangement with C_{4v} as the point symmetry of the La³⁺ site [12]. Meanwhile, the La³⁺ has the largest ionic radius among the lanthanide ions (Ln³⁺), and it can be easily substituted by

W. Yu · Q. Kong · J. Wang (✉) · X. Dong (✉) · G. Liu
Key Laboratory of Applied Chemistry and Nanotechnology at
Universities of Jilin Province, Changchun University of Science
and Technology, Changchun 130022, China
e-mail: wjx87@163.com

X. Dong
e-mail: dongxiangting888@163.com

different Ln^{3+} ions in the structure [13]. Therefore, LaOCl is an excellent host for doping with various Ln^{3+} ions. In addition, LaOCl nanomaterials have aroused great interest due to their attractive properties and tremendous applications such as catalyst supports and gas sensors [14, 15]. Hence, LaOCl:Er^{3+} nanomaterials have promising applications in such fields as UC luminescence, medical diagnosis and bioimaging probes etc. It has been proven that controlled synthesis of well-defined LaOCl:Er^{3+} with uniform dimensions and morphology is of extraordinary importance because the electronic structure, bonding, surface energy, and chemical reactivity are directly related to their size and morphology [16]. Up to now, numerous efforts have been devoted to the exploration of various convenient and efficient approaches to fabricate LaOCl:Er^{3+} nanomaterials with the controlled morphology, size, and dimensionality, such as high temperature solid state reaction [11], precipitation method [17], hydrothermal–solvothermal method [18], sol–gel method [19] and precursor thermal decomposition method [20]. Electrospinning technology has been extensively explored as a simple and versatile method for forming inorganic superfine nanomaterials using polymer/inorganic composite as the precursor [21, 22]. The morphology of nanomaterials prepared by electrospinning can be controlled by adjusting experimental conditions, such as the viscosity of spinning solution, relative air humidity, the structure of spinneret, spinning voltage, and the distance between the spinneret and the collector [23, 24]. Nevertheless, the fabrication of LaOCl:Er^{3+} nanostructures via electrospinning combined with a double-crucible chlorination technique is not reported in the literatures. Herein, LaOCl:Er^{3+} nanostructures were successfully fabricated by double-crucible chlorination of the pre-products which were prepared by calcining the electrospun polyvinyl pyrrolidone (PVP)/ $[\text{La}(\text{NO}_3)_3+\text{Er}(\text{NO}_3)_3]$ composites, the morphology, structure, UC luminescence, near-infrared luminescent performances, the luminescent mechanism of LaOCl:Er^{3+} nanostructures were investigated in detail, and some meaningful results were obtained.

2 Experimental sections

2.1 Chemicals

Polyvinyl pyrrolidone (PVP, $M_w = 90,000$, AR), lanthanum oxide (La_2O_3 , 99.99 %) and erbium oxide (Er_2O_3 , 99.99 %) were purchased from Kemiou Chemical Co. Ltd. N, N-dimethylformamide (DMF, AR) was bought from Tiantai Chemical Co. Ltd. Nitric acid (AR) and ammonium chloride (NH_4Cl , AR) were purchased from Tianjin Renmin Chemical Co. Ltd. All chemicals were directly used as received without further purification.

2.2 Fabrication of LaOCl:x \%Er^{3+} nanofibers via electrospinning combined with chlorination technique

LaOCl:x \%Er^{3+} [$x = 0.5, 1, 3, 5$ and 7 ; x stands for molar ratio of $\text{Er}^{3+}/(\text{Er}^{3+}+\text{La}^{3+})$] nanofibers were prepared by calcinating and chloridizing the electrospun PVP/ $[\text{La}(\text{NO}_3)_3+\text{Er}(\text{NO}_3)_3]$ composite nanofibers. In the typical procedure of preparing representative LaOCl:5 \%Er^{3+} nanofibers, 0.9486 g La_2O_3 and 0.0586 g Er_2O_3 were dissolved in dilute HNO_3 (1:1, volume ratio) at elevated temperature, and mixed rare earth nitrates were obtained by removing the water from the solution by heating. The mixed rare earth nitrates were dissolved in 16.0018 g of DMF, and then 2.0001 g of PVP was added into the above solution under stirring for 6 h to form homogeneous transparent spinning solution. In the spinning solution, the mass ratios of rare earth nitrates, DMF and PVP were equal to 10:80:10. Subsequently, the spinning solution was electrospun under the high-voltage of 12.40 kV, and the distance between the spinneret and collector was fixed at 18 cm. The room temperature was 20–24 °C and the relative humidity was 30–40 %. In this way, the electrospun PVP/ $[\text{La}(\text{NO}_3)_3+\text{Er}(\text{NO}_3)_3]$ composite nanofibers were formed on the collector. As-spun nanofibers were pre-fired at 600 °C for 4 h with a heating rate of 1 °C/min in air, then the calcination temperature was decreased to 200 °C at a rate of 1 °C/min, followed by natural cooling down to room temperature, and the pre-products were acquired. LaOCl:5 \%Er^{3+} nanofibers could be fabricated by chloridizing pre-products using NH_4Cl powders as a chlorination agent. Some NH_4Cl powders were put into a small crucible, and carbon rods were loaded on the NH_4Cl powders, pre-products were placed on the carbon rods, then the small crucible was placed into a big crucible, and excess NH_4Cl powders were added into the space between the two crucibles, and the big crucible was covered with its lid. The crucibles were annealed at a rate of 1 °C/min and remained for 4 h at 600 °C, then the calcination temperature was decreased to 200 °C at a rate of 1 °C/min, and then down to room temperature naturally. We call this process as a double-crucible chlorination technique. LaOCl:5 \%Er^{3+} nanofibers were obtained via the above synthesis process. Other series of LaOCl:x \%Er^{3+} ($x = 0.5, 1, 3$ and 7) nanofibers were prepared by the similar procedure except for different doping molar concentration of Er^{3+} ions.

2.3 Preparation of LaOCl:x \%Er^{3+} nanobelts via electrospinning combined with chlorination technique

LaOCl:x \%Er^{3+} ($x = 0.5, 1, 3, 5$ and 7) nanobelts were prepared by calcinating and chloridizing the electrospun

PVP/[La(NO₃)₃+Er(NO₃)₃] composite nanobelts. In the typical procedure of preparing representative LaOCl:5 %Er³⁺ nanobelts. Rare earth nitrates were prepared by dissolving 0.8538 g La₂O₃ and 0.0527 g Er₂O₃ in dilute HNO₃ (1:1, volume ratio) and evaporating the excess water at elevated temperature, then the obtained rare earth nitrates were dissolved in 14.6058 g of DMF, and then 3.6008 g of PVP was added into the above solution under stirring for 12 h to form homogeneous transparent spinning solution. In the spinning solution, the mass ratios of rare earth nitrates, DMF and PVP were equal to 9:73:18. Subsequently, the spinning solution was electrospun under the high-voltage of 6.5 kV, and the distance between the spinneret and collector was fixed at 11 cm. The room temperature was 20–24 °C and the relative humidity was 30–40 %. In this way, the electrospun PVP/[La(NO₃)₃+Er(NO₃)₃] composite nanobelts were formed on the collector. Similar procedure was adopted to produce LaOCl:x %Er³⁺ nanobelts via chlorination of the obtained pre-products using a double-crucible chlorination technique, as described in Sect. 2.2. Other series of LaOCl:x %Er³⁺ (x = 0.5, 1, 3 and 7) nanobelts were prepared by the similar procedure except for different doping molar concentration of Er³⁺ ions.

2.4 Characterization methods

X-ray diffraction (XRD) measurements were carried out using a Rigaku D/max-RA X-ray diffractometer with Cu K α radiation of 0.15406 nm. The size and morphology of the products were observed by an XL-30 field emission scanning electron microscope (SEM) made by FEI Company. The purity of the products was examined by an OXFORD ISIS-300 energy dispersive spectrometer (EDS). Transmission electron microscope (TEM) analysis was performed using a JEM-2010 TEM under a working voltage of 200 kV. The photoluminescence spectra of the samples were recorded with a Hitachi F-7000 fluorescent spectrophotometer using a power-tunable 980-nm diode laser and a RPM2000S fast mapping instrument using YAG:Nd³⁺ (532 nm) laser as the excitation source. The specific surface areas of the nanostructures were measured by a V-Sorb 2800P specific surface area and pore size analyzer made by Gold APP Instrument Corporation.

3 Results and discussion

3.1 XRD analysis

The representative XRD patterns of LaOCl:5 %Er³⁺ nanobelts annealed at 500, 600, 700 and 800 °C for 4 h are shown in Fig. 1a. When the sample was obtained at

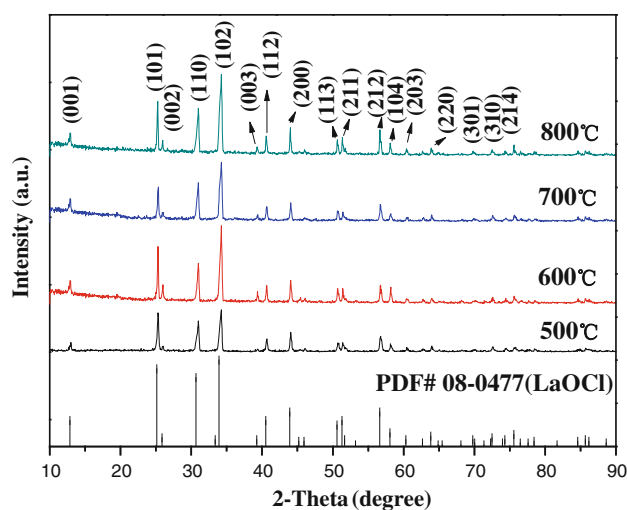


Fig. 1 XRD patterns of the LaOCl:5 %Er³⁺ nanofibers calcined at different temperatures with PDF standard card of LaOCl

500 °C, all the diffraction peaks are acquired with the low crystallinity. For the sample annealed at 600 °C, well defined diffraction peaks are acquired, and all diffraction peaks of the sample can coincide well with the tetragonal phase of LaOCl according to the PDF standard card No.08-0477. The LaOCl has PbFCl-type structure with the space group P4/nmm. Obvious diffraction peaks are situated near $2\theta = 25.50(101)$, $30.85(110)$, $34.10(102)$, $40.60(112)$, $44.20(200)$, $50.90(113)$, $51.60(211)$, $56.5(212)$, $75.70(214)$. With increasing in the annealing temperature to 700 °C and to 800 °C, diffraction peaks of the sample do not obviously change. Therefore, the optimum calcination temperature is 600 °C. Figure 2a shows the XRD patterns of the LaOCl:x %Er³⁺ nanofibers doped with different molar concentration of Er³⁺ ions calcinated at 600 °C for 4 h. No other impurity phase can be detected at the current doping concentrations, indicating that the Er³⁺ ions are completely inserted into the LaOCl host lattice through replacing the La³⁺ ions. However, the diffraction peaks are shifted to the high diffraction angle with the increase of Er³⁺ contents (as shown in the insets of Fig. 2a), meaning that the lattice constants of LaOCl:x %Er³⁺ nanofibers are changed. This is because the radius of the Er³⁺ is smaller than that of the La³⁺ [radius (La³⁺) = 1.15 Å, radius (Er³⁺) = 0.96 Å]. The lattice constants were calculated using the following expression:

$$\sin^2 \theta = (\lambda/2a)^2 \times (h^2 + k^2) + (\lambda/2c)^2 \times l^2,$$

where λ value is 1.5406 Å, h, k and l are diffraction indexes, and the results are summarized in Table 1. Similarly, the XRD results of the LaOCl:x %Er³⁺ nanobelts are manifested in Fig. 2b. It is found that the diffraction peaks of LaOCl:x %Er³⁺ nanobelts are shifted to the high diffraction angle with the increase of Er³⁺ ions contents, as

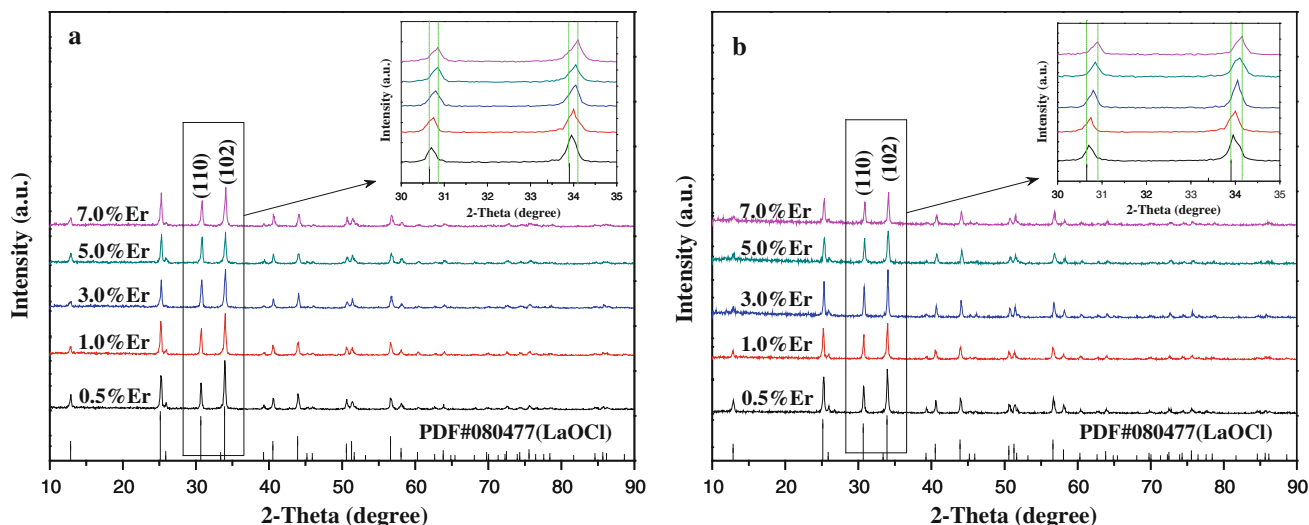


Fig. 2 XRD patterns of the LaOCl:*x* %Er³⁺ (*x* = 0.5, 1, 3, 5 and 7) nanofibers (a) and nanobelts (b) with PDF standard card of LaOCl

Table 1 Lattice constants of LaOCl:*x* %Er³⁺ (*x* = 0.5, 1, 3, 5 and 7) nanofibers

<i>x</i>	2-Theta (degree)	h	k	l	Lattice constants (Å)
0.5	30.70	1	1	0	<i>a</i> = <i>b</i> = 4.1152
	33.95	1	0	2	<i>c</i> = 6.8760
1.0	30.75	1	1	0	<i>a</i> = <i>b</i> = 4.1087
	34.00	1	0	2	<i>c</i> = 6.8670
3.0	30.80	1	1	0	<i>a</i> = <i>b</i> = 4.1022
	34.05	1	0	2	<i>c</i> = 6.8579
5.0	30.85	1	1	0	<i>a</i> = <i>b</i> = 4.0957
	34.10	1	0	2	<i>c</i> = 6.8489
7.0	30.90	1	1	0	<i>a</i> = <i>b</i> = 4.0893
	34.15	1	0	2	<i>c</i> = 6.8400

indicated in the inset of Fig. 2b. The diffraction angles of LaOCl:*x* %Er³⁺ nanobelts are same with the counterpart nanofibers, indicating that they have same structures.

3.2 Morphology observations

Figure 3 shows the representative SEM images of the LaOCl:5 %Er³⁺ nanofibers and nanobelts. From the SEM image of Fig. 3a, it can be noticed that the LaOCl:5 %Er³⁺ nanofibers have coarse surface with good dispersity. The SEM image of the LaOCl:5 %Er³⁺ nanobelts with the thickness of 116 nm (shown in the inset of Fig. 3b) is manifested in Fig. 3b, they were relatively smooth. Under the 95 % confidence level, the diameter of LaOCl:5 %Er³⁺ nanofibers and width of the nanobelts analyzed by Shapiro–Wilk method are normal distribution. Histograms of diameter and width distribution of the nanostructures are indicated in Fig. 4. As seen from Fig. 4, the diameter of the

LaOCl:Er³⁺ nanofibers is 161.15 ± 18.11 nm, the width and thickness of the nanobelts are 6.11 ± 0.19 μm and 116 nm, respectively. TEM images of the LaOCl:5 %Er³⁺ nanofibers and nanobelts are presented in Fig. 5. It is found that LaOCl:5 %Er³⁺ nanofibers and nanobelts are composed of nanoparticles, and the diameter of LaOCl:5 %Er³⁺ nanofibers and the width of nanobelts are ca. 160 nm and 6.1 μm, respectively. The results are consistent with the results of SEM analysis.

Figure 6 indicates the EDS spectra of the PVP/[La(NO₃)₃+Er(NO₃)₃] composite nanofibers and LaOCl:5 %Er³⁺ nanofibers. EDS spectra show that C, N, O and La, Er are the main elements in composite nanofibers, Cl, O, Er and La in LaOCl:5 %Er³⁺ nanofibers, and the same results are obtained for composite nanobelts and LaOCl:5 %Er³⁺ nanobelts. Au comes from the conductive film coated on samples for SEM observation. No other elements are found in the samples, indicating that the LaOCl:Er³⁺ nanostructures are highly pure.

3.3 Upconversion luminescence properties

Figure 7 shows the UC emission spectra of LaOCl:*x* %Er³⁺ (*x* = 0.5, 1, 3, 5 and 7) nanofibers and nanobelts under the excitation of a 980-nm DL with the same pump power (in order to avoid the experimental errors). The UC emission spectra consist of red emission bands and green emission bands. The red emission bands centering at 671 nm originate from ⁴F_{9/2} → ⁴I_{15/2} transition of Er³⁺ ions, and the green emission peaks at 525 nm, 548 nm are ascribed to the ²H_{11/2}, ⁴S_{3/2} → ⁴I_{15/2} energy levels transitions of Er³⁺ ions, respectively. It is found that the spectral shape and position of excitation and emission peaks do not vary with the doping concentrations of Er³⁺ ions for

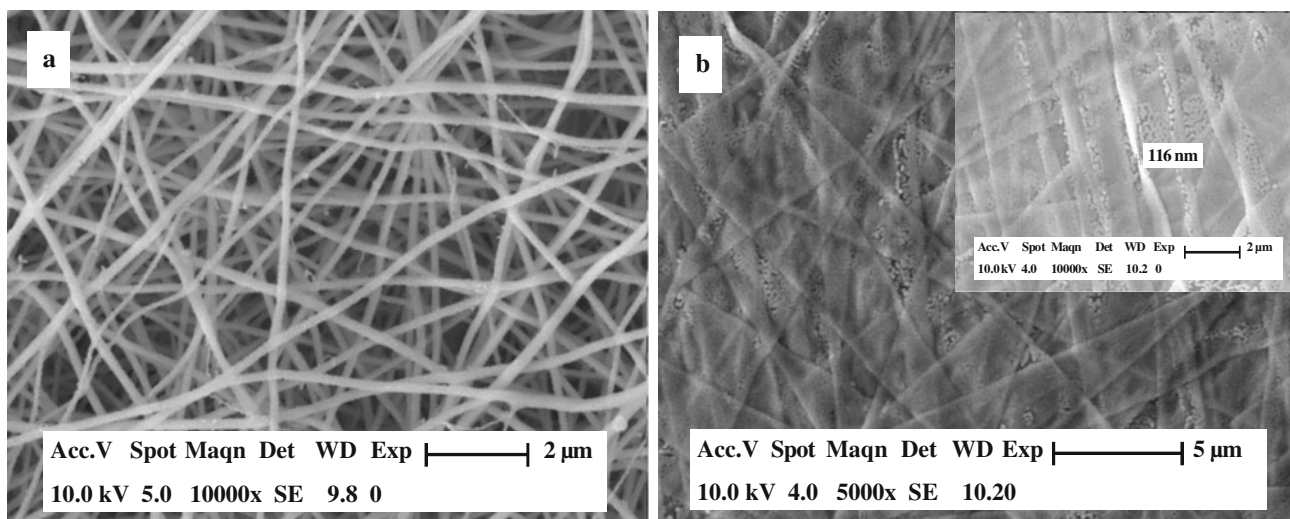


Fig. 3 SEM images of LaOCl:5 %Er³⁺ nanofibers (a) and nanobelts (b)

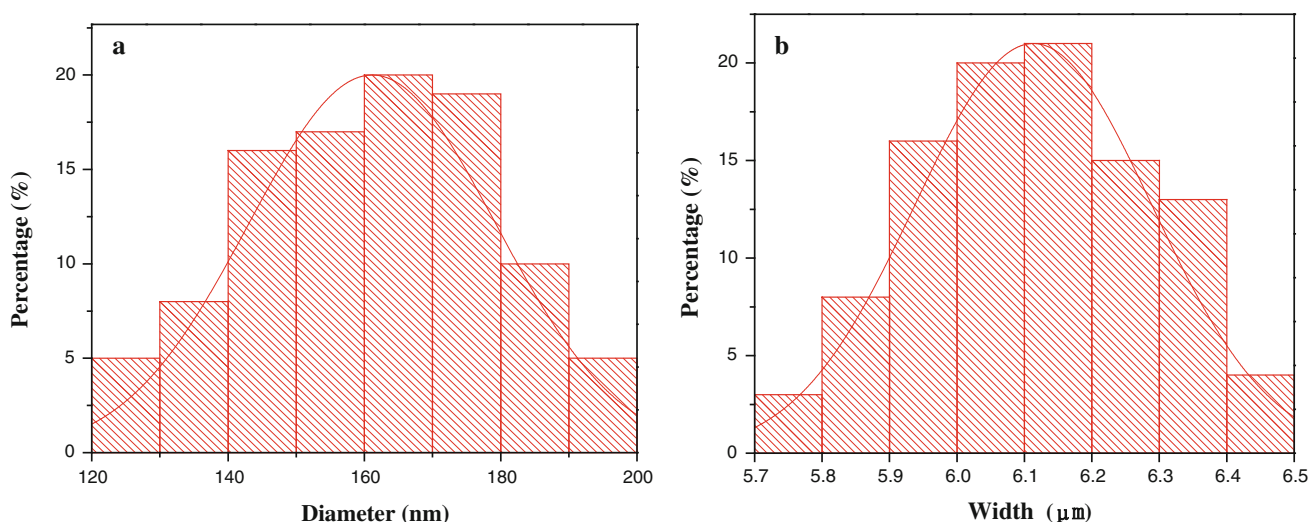


Fig. 4 Histograms of diameter distribution of LaOCl:5 %Er³⁺ nanofibers (a) and width distribution of LaOCl:5 %Er³⁺ nanobelts (b)

LaOCl:*x* %Er³⁺ nanostructures, however, the intensity of excitation and emission peaks for LaOCl:*x* %Er³⁺ nanostructures strongly depends on the doping concentration of Er³⁺ ions. The dependence of the intensity of the emission peaks (both green and red emission) on Er³⁺ ions concentration in LaOCl:*x* %Er³⁺ nanofibers and nanobelts are shown in Fig. 8a, b, respectively. It can be seen that the emission peaks intensity increases with Er³⁺ ions concentration from 0.5 to 5 % and decreases with further increasing in the Er³⁺ ions concentration from 5 to 7 %. The results can be interpreted by the internal concentration quenching. The concentration quenching mechanism is generally associated with ET. Non-radiative ET process from a Er³⁺ ion to another Er³⁺ ion may be described by three different methods: (1) exchange interaction; (2)

radiation reabsorption; (3) multipolar interaction [25]. While considering the mechanism of ET in LaOCl:Er³⁺ nanostructures, the concentration quenching can be explained in more detail by critical distance (*R_c*), and the critical distance (*R_c*) between Er³⁺ ions for ET can be calculated using the formula that was proposed by Blasse and Grabmaier as below [26]:

$$R_c = 2 \times (3V/4\pi X_c N)^{1/3}$$

where *V* is the volume of the unit cell, *X_c* is the critical concentration of activator ions, and *N* is the number of formula available crystallographic sites occupied by the activator ions in the unit cell. In case of LaOCl:Er³⁺ nanostructures, *X_c* = 0.05, *V* = 0.1149 nm³, and *N* = 4. Therefore, the average distance *R_c* between Er³⁺ ions is

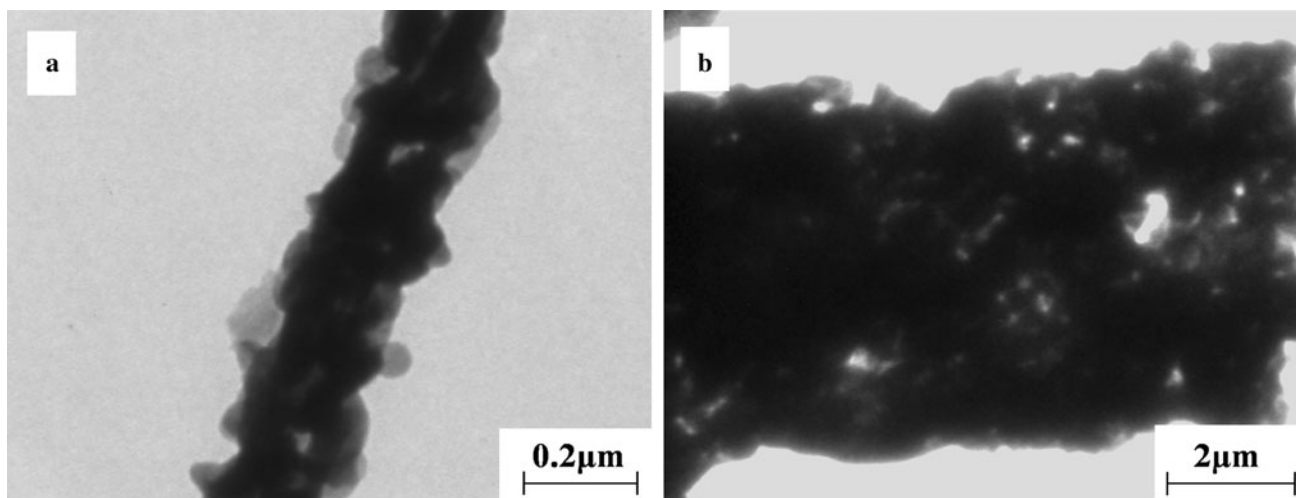


Fig. 5 TEM images of LaOCl:5 %Er³⁺ nanofibers (a) and nanobelts (b)

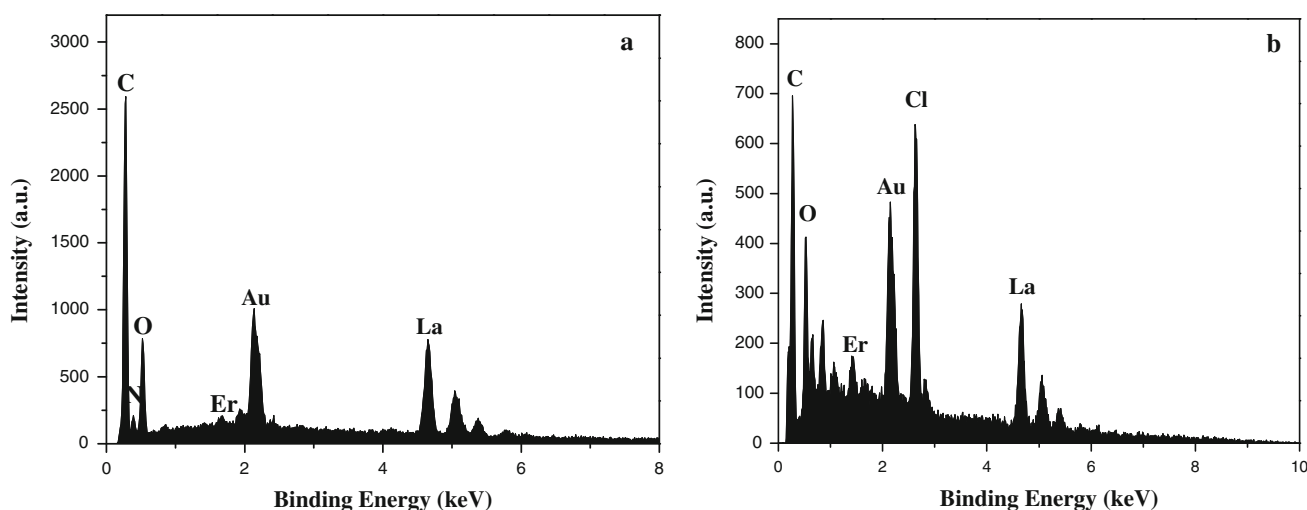


Fig. 6 EDS spectra of PVP/[La(NO₃)₃+Er(NO₃)₃] composite nanofibers (a) and LaOCl:5 %Er³⁺ nanofibers (b)

calculated to be 1.0314 nm. The ratio of green to red emission intensity ($f_{g/r}$) monotonously decreases with Er³⁺ concentration from 0.5 to 7 %. The $f_{g/r}$ of the LaOCl: x %Er³⁺ ($x = 0.5, 1, 3, 5$ and 7) nanofibers respectively are 5.46, 4.92, 2.60, 1.40 and 1.27, as shown in Fig. 8c. Similarly, the $f_{g/r}$ of the LaOCl: x %Er³⁺ ($x = 0.5, 1, 3, 5$ and 7) nanobelts respectively are 4.88, 4.19, 1.63, 1.40 and 1.22, as shown in Fig. 8d.

For comparison, the UC emission spectra of LaOCl:5 %Er³⁺ nanofibers and nanobelts under the excitation of a 980-nm DL with the same pump power are shown in Fig. 9. It can be found that the nanobelts have higher UC emission (both red and green) intensity than the nanofibers. It is known that the specific surface area of materials increases with the decrease of size [27]. A large number of defects are introduced into LaOCl:5 %Er³⁺ nanostructures

due to the large surface area. Defects as quenching centers have severe drawback for luminescence intensity of nanomaterials because they provide nonradiative recombination centers for electrons and holes [28]. The BET specific surface areas of LaOCl:5 %Er³⁺ nanofibers and nanobelts are determined to be 27.52 and 15.29 m²/g. Therefore, LaOCl:5 %Er³⁺ nanobelts have the smaller quantity of defects due to the smaller specific surface area than the nanofibers, as a result, the nanobelts have stronger UC luminescence intensity than the nanofibers. The same phenomena are obtained for other series of LaOCl: x %Er³⁺ ($x = 0.5, 1, 3$ and 7) nanostructures.

To understand the physical mechanisms of the UC luminescence described above, especially the prominent enhancement of red UC emission, the emission intensities were measured as a function of the pump power to

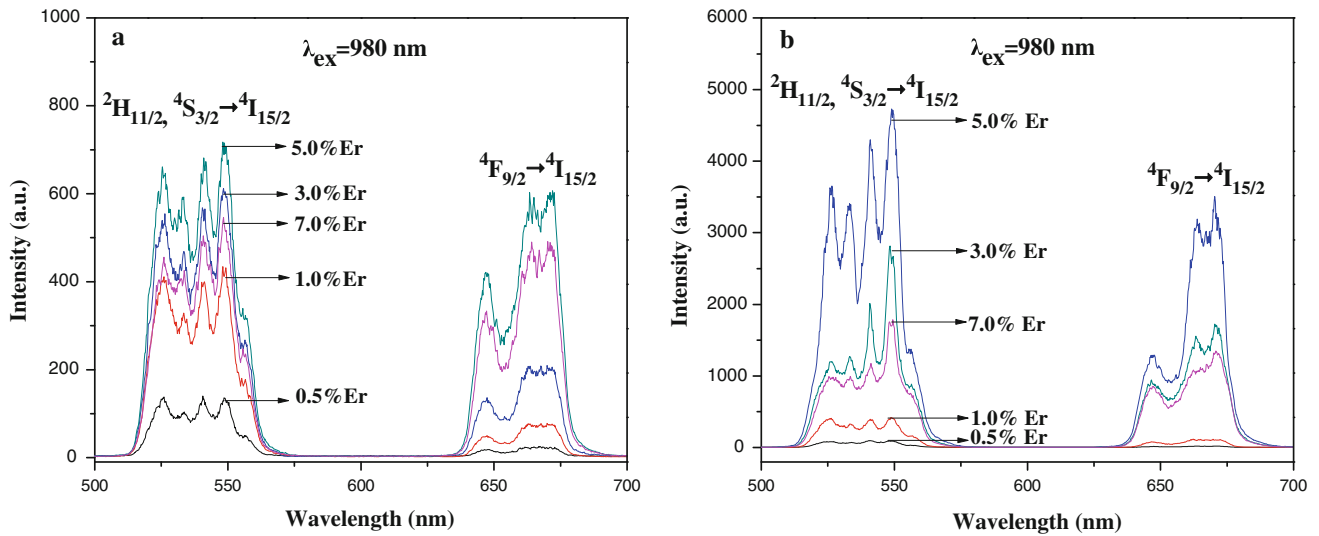


Fig. 7 UC emission spectra of LaOCl: x %Er $^{3+}$ ($x = 0.5, 1, 3, 5$ and 7) nanofibers (a) and nanobelts (b)

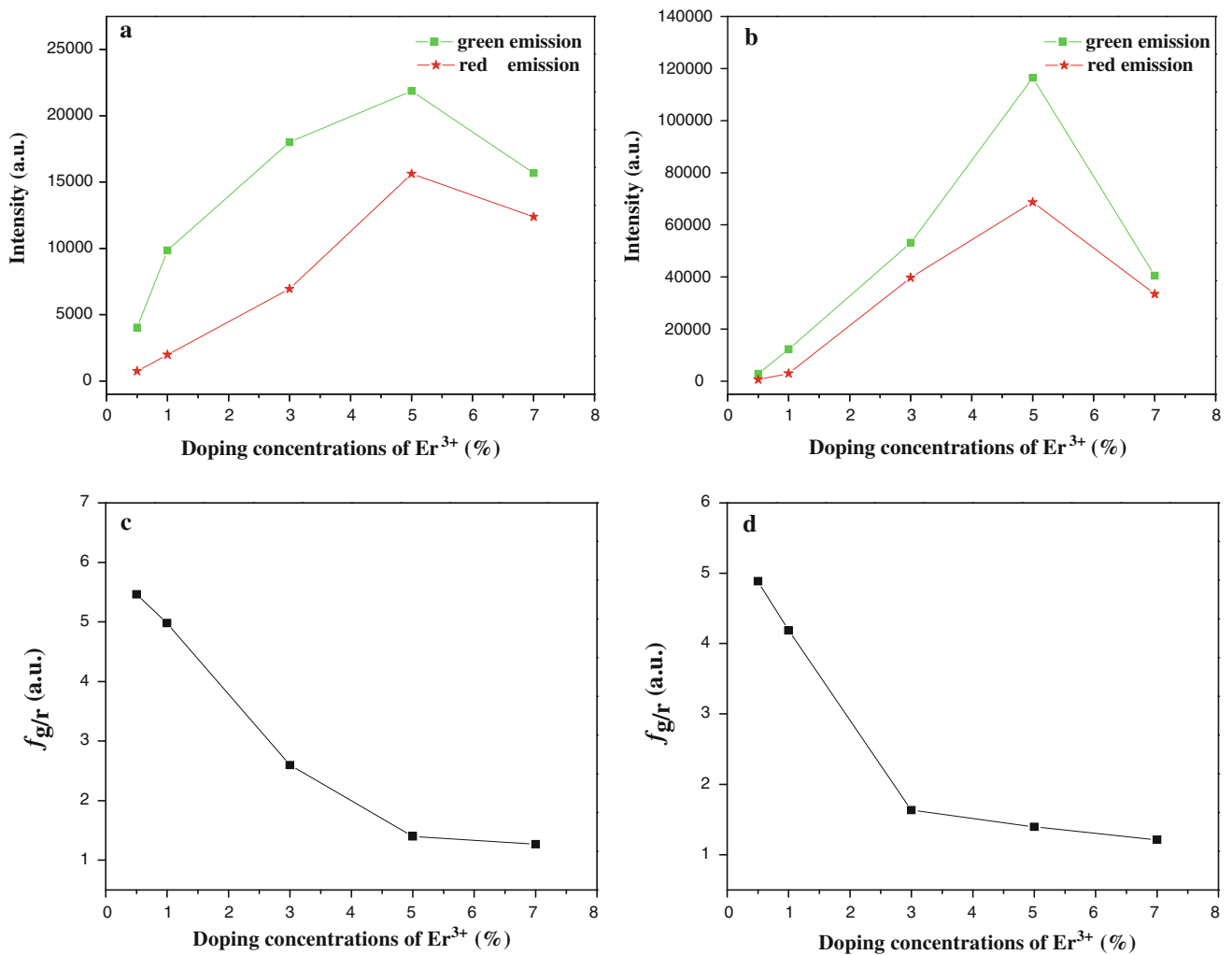


Fig. 8 Dependence of the emission intensities on doping concentration and the intensity ratio I_{green}/I_{red} for LaOCl: x %Er $^{3+}$ ($x = 0.5, 1, 3, 5$ and 7) nanofibers (a, c) and nanobelts (b, d) under the excitation of a 980-nm DL. Square (■) stands for green emission; star (★) stands for red emission (Color figure online)

determine the number of the photons responsible for the visible emission. For the upconversion process, the up-converted emission intensity (I_{up}) depends on the pump power (P) according to the following relation:

$$I_{up} \propto P^n$$

where n is the number of pump photons required. Figure 10a shows the UC emission spectra of the LaOCl:5 %Er³⁺ nanofibers under the excitation of a 980-nm DL with different pump power. A plot of natural logarithm I_{up} versus natural logarithm P^n pump yields a straight line with slope n , as shown in Fig. 10b. It can be seen that the slopes (values of n) obtained are 1.94 and 1.95 for the green emission transition (²H_{11/2}, ⁴S_{3/2} → ⁴I_{15/2}) and red emission transition (⁴F_{9/2} → ⁴I_{15/2}), respectively. Generally, a straight line with

the slope ~ 2 for the upconversion luminescence indicates that two photons involve in this upconversion luminescence process. Therefore, our results reveal that two photons process should be mainly responsible for the green and red emissions of the LaOCl:5 %Er³⁺ nanofibers, and the green UC emission is predominant. Similarly, the UC emission spectra of LaOCl:5 %Er³⁺ nanobelts under the excitation of a 980-nm DL with different pump power are shown in Fig. 11a, and the natural logarithmic plots of the UC emission intensities as a function of the pump power are also given in Fig. 11b. The values of n for the UC luminescence of the red emission transition (⁴F_{9/2} → ⁴I_{15/2}) and the green emission transition (²H_{11/2}, ⁴S_{3/2} → ⁴I_{15/2}) are 1.92 and 2.25, respectively. It is clearly found that the two-photon process contributes to the red and green emission, and the green UC emission is predominant.

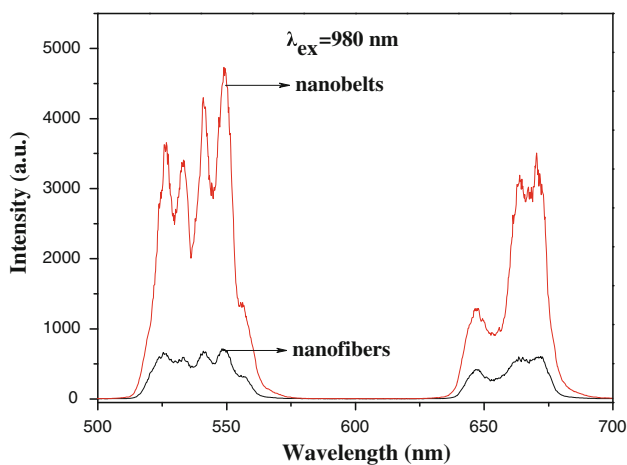


Fig. 9 UC emission spectra of LaOCl:5 %Er³⁺ nanofibers and nanobelts

3.4 Upconversion luminescent mechanisms of LaOCl:Er³⁺ nanostructures

In principle, four basic population mechanisms may be involved in the UC process, namely ground state absorption (GSA), excited state absorption (ESA), ET and PA [11, 29]. We can immediately rule out PA as a mechanism of UC in LaOCl:Er³⁺ nanostructures because no inflection point was observed in the power study. The ET process can be excluded because no sensitizer in the system. The two photon process in LaOCl:Er³⁺ nanostructures may happen via the following GSA and ESA processes, and their possible schematic diagram is shown in Fig. 12. It can be seen that Er³⁺ ions are excited from the ground state to the ⁴I_{11/2} state by GSA, then the ions in ⁴I_{11/2} level rise to ⁴F_{7/2} level via the ESA. The Er³⁺ ions at ⁴F_{7/2} level undergo multi-phonon relaxation to the green luminescent ²H_{11/2} and ⁴S_{3/2}

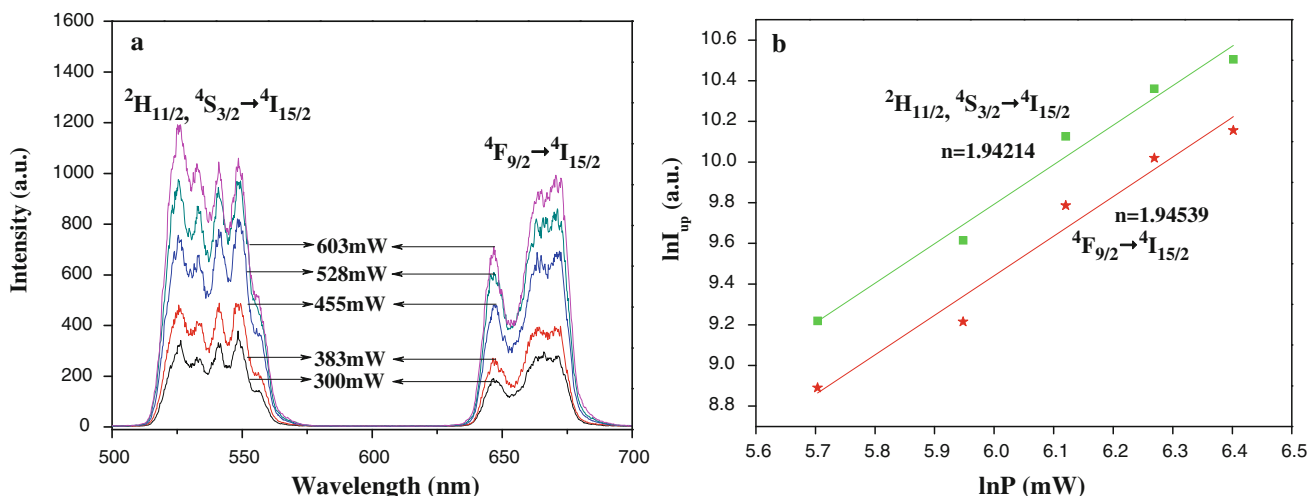


Fig. 10 UC emission spectra under the excitation of a 980-nm DL (a) and the plots of natural logarithmic intensities of the UC emission (I_{up}) versus natural logarithmic pump power (P) of a 980-nm DL (b) for LaOCl:5 %Er³⁺ nanofibers

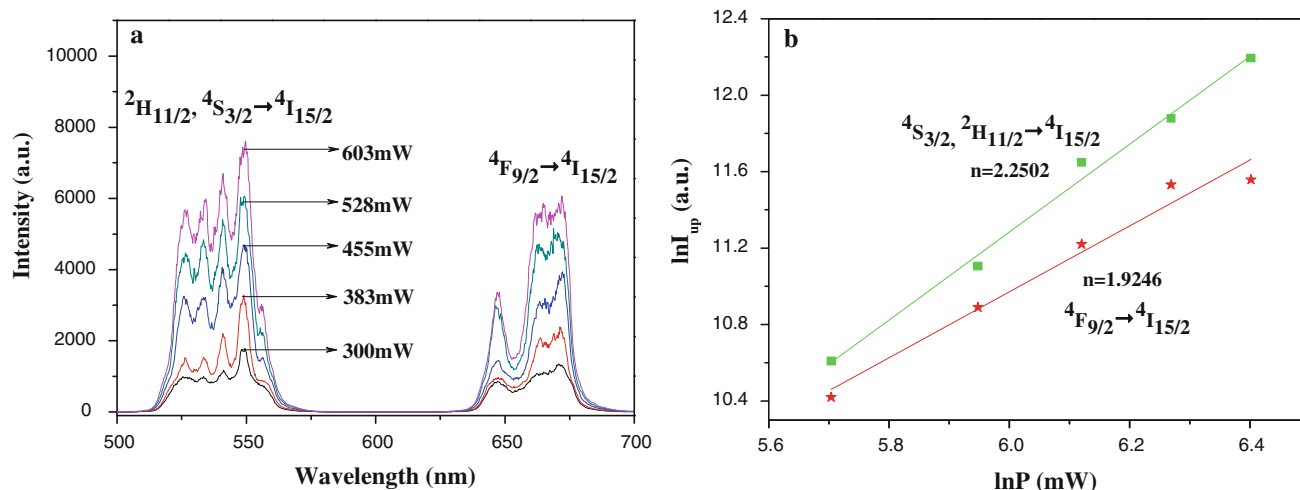


Fig. 11 UC emission spectra under the excitation of a 980-nm DL (a) and the plots of natural logarithmic intensities of the UC emission (I_{up}) versus natural logarithmic pump power (P) of a 980-nm DL (b) for LaOCl:5 %Er³⁺ nanobelts

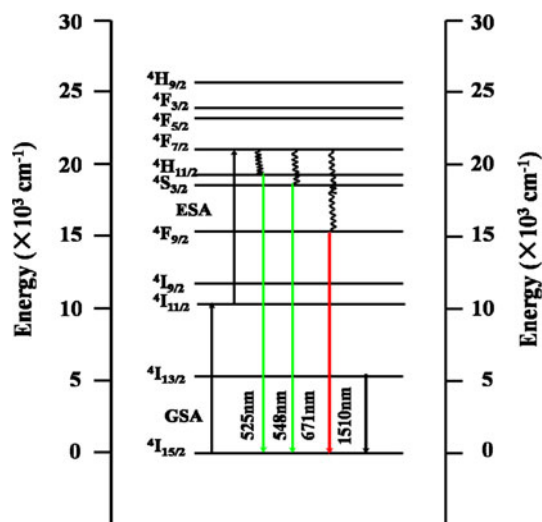


Fig. 12 Simplified energy level scheme of the UC emission mechanism for Er³⁺-doped LaOCl nanostructures

levels, and the green emission bands are yielded through the transitions of $^4S_{3/2} \rightarrow ^4I_{15/2}$ and $^2H_{11/2} \rightarrow ^4I_{15/2}$. The red emission bands centered at 671 nm originate from the transition from the $^4F_{9/2}$ to $^4I_{15/2}$, as the $^4F_{7/2}$ and $^4F_{9/2}$ levels are separated by a relatively high energy gap, the possibility for the thermal relaxation between them will be low. Therefore, the intensity of red emission peaks is weaker than that of green emission peaks.

3.5 Near-infrared luminescence analysis

Figure 13 shows the near-infrared emission spectra around 1.51 μ m for LaOCl: x %Er³⁺ ($x = 0.5, 1, 3, 5$ and 7) nanofibers, nanobelts and LaOCl:5 %Er³⁺ nanostructures

with different morphology under the excitation of a 532-nm laser. The Er³⁺ ions are promoted to the excited state $^4I_{11/2}$ from the ground state $^4I_{15/2}$ by GSA process. The electrons in $^4I_{13/2}$ level are achieved by non-radiative relaxation from $^4I_{11/2}$ level and give the characteristic emission at 1.51 μ m via the radiative transition from $^4I_{13/2}$ state to ground state. In addition, the spectral shape and position of emission peaks do not vary with the doping concentration of Er³⁺ ions and morphologies of nanomaterials, but the intensity of emission peaks strongly depends on the doping concentration of Er³⁺ ions and morphologies of nanomaterials. In summary, the strongest emission spectra can be obtained when the doping molar concentration of Er³⁺ ions is 5 % for LaOCl: x %Er³⁺ nanofibers and nanobelts, as revealed in Fig. 13a, b. The nanobelts have higher near-infrared emission intensity than the nanofibers, as shown in Fig. 13c.

3.6 CIE analysis

Generally, color is represented by the Commission Internationale de L'Eclairage (CIE) chromaticity coordinates and color ratios. The chromaticity coordinates have been calculated from the emission spectra by the method described in previous paper [30]. For the LaOCl: x %Er³⁺ ($x = 0.5, 1, 3, 5$ and 7) nanofibers, the chromaticity coordinates (X, Y) are determined to be [(0.256, 0.663), (0.246, 0.717), (0.261, 0.702), (0.294, 0.674) and (0.301, 0.646)], which correspond to the Er³⁺ concentration of 0.5, 1, 3, 5 and 7 %, respectively. Obviously, the emission colors of LaOCl: x %Er³⁺ nanofibers are obviously green to the naked eye, as shown in Fig. 14a. Similarly, CIE chromaticity coordinates diagram for LaOCl: x %Er³⁺ ($x = 0.5, 1, 3, 5$ and 7) nanobelts was shown in Fig. 14b.

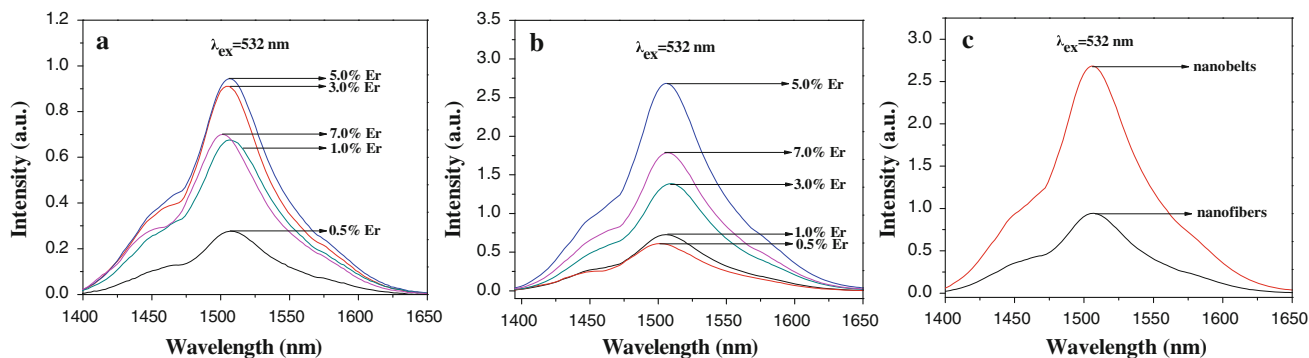


Fig. 13 Near-infrared emission spectra of LaOCl:*x* %Er³⁺ (*x* = 0.5, 1, 3, 5 and 7) nanofibers (a), nanobelts (b) and LaOCl:5 %Er³⁺ nanostructures with different morphology (c) under the excitation of a 532-nm laser

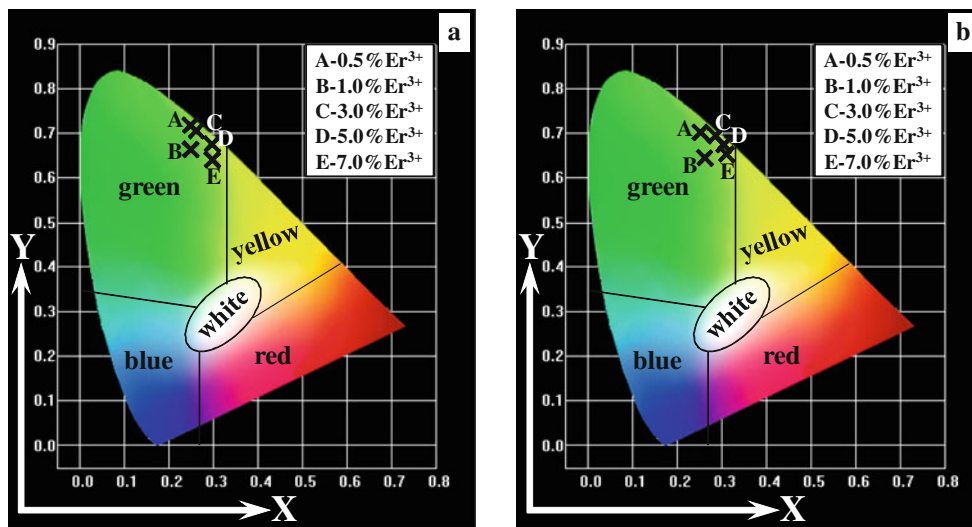


Fig. 14 CIE chromaticity coordinates diagrams for LaOCl:*x* %Er³⁺ (*x* = 0.5, 1, 3, 5 and 7) nanofibers (a) and nanobelts (b)

Their emission colors appear in the green region, and the chromaticity coordinates (X, Y) are [(0.263, 0.641), (0.255, 0.703), (0.284, 0.694), (0.306, 0.671) and (0.311, 0.656)], which correspond to the Er³⁺ concentration of 0.5, 1, 3, 5 and 7 %, respectively. According to the above results, it can be found that the emission colors of LaOCl:*x* %Er³⁺ nanomaterials can be tuned by changing the concentration of Er³⁺ ions, which is considered to be a promising candidate for application in LEDs.

4 Conclusions

One-dimensional pure tetragonal phase LaOCl:Er³⁺ nanofibers and nanobelts have been successfully synthesized by electrospinning technique in conjunction with a double-crucible chlorination technique. The diameter of the LaOCl:Er³⁺ nanofibers is 161.15 ± 18.11 nm, the width and thickness of the nanobelts are 6.11 ± 0.19 μm and

116 nm, respectively. Under the excitation of a 980-nm DL, LaOCl:Er³⁺ nanostructures exhibit the green and red UC emissions centering at 525 nm, 548 nm and 671 nm, respectively attributed to ²H_{11/2} → ⁴I_{15/2}, ⁴S_{3/2} → ⁴I_{15/2} and ⁴F_{9/2} → ⁴I_{15/2} transitions of Er³⁺. The relative intensities of green and red emissions vary obviously with the addition of Er³⁺ ions, and the optimum molar percentage of Er³⁺/(La³⁺+Er³⁺) ions was 5 % in the LaOCl:Er³⁺ nanostructures. The LaOCl:*x* %Er³⁺ nanobelts have higher UC emission (both red and green) intensity than the counterpart nanofibers. The near-infrared characteristic emission of predominant peak at 1.51 μm of LaOCl:Er³⁺ nanostructures is achieved under the excitation of a 532-nm laser. Color-tuned luminescence can be obtained by changing the doping concentration of Er³⁺ ions.

Acknowledgments This work was financially supported by the National Natural Science Foundation of China (NSFC 50972020, 51072026), Ph.D. Programs Foundation of the Ministry of Education of China (20102216110002, 20112216120003), the Science and

Technology Development Planning Project of Jilin Province (Grant Nos. 20130101001JC, 20070402, 20060504), the Science and Technology Research Project of the Education Department of Jilin Province during the eleventh five-year plan period (Under Grant No. 2010JYT01), Key Research Project of Science and Technology of Ministry of Education of China (Grant No. 207026).

References

1. M. Haase, H. Schäfer, *Angew. Chem. Int. Ed.* **50**, 5808–5829 (2011)
2. F. Wang, Y. Han, C.S. Lim, Y.H. Lu, J. Wang, J. Xu, H.Y. Chen, C. Zhang, M.H. Hong, X.G. Liu, *Nature* **463**, 1061–1065 (2010)
3. D.Q. Chen, Y.L. Yu, F. Huang, A.P. Yang, Y.S. Wang, *J. Mater. Chem.* **21**, 6186–6192 (2011)
4. J. Dinga, Q. Zhang, J.M. Cheng, X.F. Liu, G. Lin, J.R. Qiu, D.P. Chen, *J. Alloys Compd.* **495**, 205–208 (2010)
5. F. Wang, X.G. Liu, *Chem. Soc. Rev.* **38**, 976–989 (2009)
6. T. Konishi, M. Shimizu, Y. Kameyama, K. Soga, *J. Mater. Sci.: Mater. Electron.* **18**, 183–186 (2007)
7. C.X. Li, J. Lin, *J. Mater. Chem.* **20**, 6831–6847 (2010)
8. Y. Li, X.T. Wei, M. Yin, *J. Alloys Compd.* **509**, 9865–9868 (2011)
9. L.Q. An, J. Zhang, M. Liu, S.W. Wang, *J. Alloys Compd.* **451**, 538–541 (2008)
10. L.A. Riseberg, H.W. Moos, *Phys. Rev.* **174**, 429–438 (1968)
11. Z.G. Xia, J. Li, Y. Luo, L.B. Liao, *J. Am. Ceram. Soc.* **95**(10), 3229–3234 (2012)
12. Y. Li, X. Wei, B. Tong, Y. Liu, Q. Zhang, W. Sun, M. Yin, *Mater. Lett.* **80**, 184–186 (2012)
13. S.S. Lee, H.I. Park, C.H. Joh, S.H. Byeon, *J. Solid State Chem.* **180**, 3529–3534 (2007)
14. A. Marsal, E. Rossinyol, F. Bimbela, C. Tellez, J. Coronas, A. Cornet, *Sens. Actuators B* **109**, 38–43 (2005)
15. E.N. Maslen, S.V.A. Treltsov, N.R. Streltsova, N. Ishizawa, *Acta Crystallogr. Sect. B: Struct. Sci.* **52**, 576–579 (1996)
16. G. Jia, H.P. You, Y.H. Song, J.J. Jia, Y.Z. Zheng, L.H. Zhang, K. Liu, H.J. Zhang, *Inorg. Chem.* **48**, 10193–10201 (2009)
17. S.G. Podkolzin, E.E. Stangland, M.E. Jones, E. Peringer, J.A. Lercher, *J. Am. Chem. Soc.* **129**, 2569–2576 (2007)
18. S.S. Lee, C.H. Joh, S.H. Byeon, *Mater. Sci. Eng., B* **151**, 163–168 (2008)
19. G.G. Li, C.X. Li, C.M. Zhang, Z.Y. Cheng, Z.W. Quan, C. Peng, J. Lin, *J. Mater. Chem.* **19**, 8936–8943 (2009)
20. Y.P. Du, Y.W. Zhang, L.D. Sun, C.H. Yan, *J. Am. Chem. Soc.* **131**, 3163–3165 (2009)
21. Q.L. Ma, J.X. Wang, X.T. Dong, W.S. Yu, G.X. Liu, J. Xu, *J. Mater. Chem.* **22**, 14438–14442 (2012)
22. W.W. Ma, X.T. Dong, J.X. Wang, W.S. Yu, G.X. Liu, *J. Mater. Sci.* **48**, 2557–2565 (2013)
23. J.M. Deitzel, J.K. Ieinmeyer, D. Harris, N.C. Tan, *Polymer* **42**, 261–272 (2001)
24. A. Greiner, J.H. Wendorff, *Angew. Chem. Int. Ed.* **46**, 5670–5703 (2007)
25. L.G. Van Uitert, *J. Electrochem. Soc.* **114**, 1048–1053 (1967)
26. G. Blasse, *Phys. Lett. A* **28**, 444–445 (1968)
27. K. Kömpe, O. Lehmann, M. Haase, *Chem. Mater.* **18**, 4442 (2006)
28. G.G. Li, Z.Y. Hou, C. Peng, W.X. Wang, Z.Y. Cheng, C.X. Li, H.Z. Lian, J. Lin, *Adv. Funct. Mater.* **20**, 3442–3453 (2010)
29. Y.H. Song, Y.J. Huang, L.H. Zhang, Y.H. Zheng, N. Guo, H.P. You, *RSC Adv.* **2**, 4777 (2012)
30. J. Ghys, R. Mauricot, B. Caillier, P. Guillot, T. Beaudette, G. Jia, P. Tanner, B. Cheng, *J. Phys. Chem. C* **114**, 6681 (2010)